Structural difference between liquidlike and gaslike phases in supercritical fluid

Takashi Sato
Graduate School of Engineering, Kyoto University, Kumatori, Osaka 590-0494, Japan

Masaaki Sugiyama,* Keiji Itoh, Kazuhiro Mori, and Toshiharu Fukunaga
Research Reactor Institute, Kyoto University, Kumatori, Osaka 590-0494, Japan

Masakatsu Misawa and Toshiya Otomo
High Energy Accelerator Research Organization (KEK), Tsukuba, Ibaraki 305-0801, Japan

Shinichi Takata
Japan Atomic Energy Agency (JAEA), Tokai, Ibaraki 319-1184, Japan
(Received 6 August 2008; published 6 November 2008)

Density fluctuation structures of supercritical carbon dioxide along the isothermal and isochoric lines were observed with small-angle neutron scattering (SANS). All the scattering intensities in the low-Q range were well described with the Ornstein-Zernike (OZ) equation. It was confirmed that there exists a locus where the OZ correlation length and scattering intensity at $Q=0$ exhibit extrema on the isothermal lines: this locus, named the ridge, was interpreted as the boundary by which the supercritical state is divided into liquidlike and gaslike phases. In order to clarify the difference of the fluctuation structure between the liquidlike and the gaslike phases, a real-space molecular distribution was obtained with a reverse Monte Carlo (RMC) method. Number density distributions of CO_2 molecules at all measured states were calculated with the real-space molecular distributions obtained. In addition, the statistical parameters of the number density distributions, the standard deviations, and the skewnesses, were examined. The standard deviations of the number density distributions almost coincide with the results of the OZ analysis. On the other hand, the skewnesses, which describe the asymmetric nature of the number density distribution, clearly showed a difference between the two phases: the skewness became negative in the liquidlike phase, positive in the gaslike phase, and almost zero at the nearest state to the ridge in all isotherms. It was proved with simple equations of statistical mechanics that the skewness is described as the first differential of the magnitude of the density fluctuation with respect to the pressure. We conclude that the skewness, obtained with a RMC analysis for SANS data, is an important structural parameter distinguishing between the liquidlike and gaslike phases.

DOI: 10.1103/PhysRevE.78.051503 PACS number(s): 61.05.fg, 61.20.−p

I. INTRODUCTION

A supercritical fluid (SCF) is generally defined as any substance at a temperature T higher than its critical temperature T_c [1]. A SCF can change its density in a wide range without a liquid-gas phase transition. The viscosity and diffusion coefficient of the fluid also vary from liquidlike to gaslike values with a small change of the thermodynamic state. Because of these features, SCFs are expected to be useful for extraction, chromatography, chemical reactions, material synthesis, and so on.

It has been considered that the chemical and physical properties of SCFs, such as solubility and compressibility, are strongly connected with their large-scale density fluctuation structure [1]. One of the most characteristic features of the density fluctuation in the supercritical phase is a "ridge" which Nishikawa and co-workers found with small-angle x-ray scattering [2–12]. The ridge is defined as the locus of the states where the scale and the magnitude of the density fluctuation become maximal on the isothermal line. The ridge is regarded as a kind of boundary which divides the supercritical region into liquidlike and gaslike phases because the solubility of the SCF changes drastically there. In addition, the magnitude of the density fluctuation is directly connected with the isothermal compressibility, which is the second derivative of the Gibbs energy. Therefore, the isothermal compressibility [13] and the other thermodynamic parameters that relate to the second derivative of the Gibbs energy, such as partial molar volume [14], sound velocity [15], and thermal conductivity [16], have extrema at the ridge.

The difference of molecular distribution structures between the liquidlike and gaslike phases has attracted much interest to understanding the solution properties of SCFs. Generally, the Ornstein-Zernike (OZ) equation is used for describing the small-angle neutron or x-ray scattering intensity $I(Q)$ of the large-scale density fluctuation structure:

$$I(Q) = \frac{I(0)}{1 + \xi^2 Q^2}, \tag{1}$$

where ξ and Q are the OZ correlation length, which corresponds to the scale of the density fluctuation, and the magnitude of the scattering vector ($Q=4\pi \sin\theta/\lambda$, where 2θ is the scattering angle and λ is the wavelength). $I(0)$, the scat-

*sugiyama@rri.kyoto-u.ac.jp

tering intensity at $Q=0$, is connected with the magnitude of the density fluctuation by the relation

$$I(0) \propto \langle N^2 \rangle - \langle N \rangle^2, \tag{2}$$

where N is the number of molecules in the corresponding volume V. The fluctuation parameters ξ and $I(0)$ symmetrically decrease away from the ridge with respect to pressure or density. However, no characteristic differences between the liquidlike and gaslike phases have been shown by OZ analysis. In the previous studies, the structural difference between the two phases was presumed to come from the difference of the scatterers in the phases, i.e., the scattering intensity reflects the distribution of the molecular aggregates in the gaslike phase, but that of voids in the liquidlike phase [10]. Nonetheless, this presumption leaves much room for argument. Because the OZ equation describes only the deviation of the local density from the average one, it cannot distinguish the difference between the aggregates and the voids. Moreover, the behavior of the solution properties mentioned above is not explained by only an analysis of the OZ equation. Therefore we have to find another structural parameter that describes the difference between the liquidlike and gaslike phases in a SCF. To accomplish the purpose, it is necessary to establish an advanced analytical method which can extract more detailed structural information from the scattering data than the traditional one.

In recent years, we have investigated the density fluctuation structure of supercritical carbon dioxide (sc-CO_2) with small-angle neutron scattering (SANS) [17–19]. In particular, by applying a reverse Monte Carlo (RMC) simulation method, the molecular distribution of sc-CO_2 was revealed in real space [18]. The RMC simulation is a kind of inverse modeling method based on the scattering data and is widely used for visualizing the local structure of disordered materials [20]. Even though the RMC method for SANS is a still developing analysis, it has the advantage of treating the real-space molecular distribution [21,22]. Therefore, it is strongly expected that there is great potential to extract more detailed structural information than in the previous analysis.

In this study, SANS experiments were performed for sc-CO_2 at more thermodynamic states than those in the previous study [18]. In particular, the structural change along both isothermal and isochoric lines was examined. Moreover, we suggest an advanced analytical method based on statistical mechanics and apply it to the real-space molecular distribution obtained with the RMC calculation. The aim of this study is to reveal the differences of the fluctuation structure between the liquidlike and gaslike phases in sc-CO_2 by applying this analysis method to the SANS data.

II. EXPERIMENTAL PROCEDURE

SANS experiments on sc-CO_2 were carried out by using the time-of-flight small- and wide-angle neutron scattering instrument (SWAN) installed at the Neutron Science Laboratory (KENS) of the High Energy Accelerator Research Organization (KEK) in Tsukuba, Japan [23]. SANS intensities were measured in 20 thermodynamic states. These measurement points are displayed on a pressure-temperature phase diagram (Fig. 1), and the thermodynamic parameters (pressure P, temperature T, and density ρ) are listed in Table I. The density in the table was calculated with the equation of state of CO_2 [24]. The deviations of temperature and pressure during the measurements were kept within ± 0.2 °C and ± 0.03 MPa, respectively. Among the 20 measurement points, the state groups (a,b,c,d,e), (f,g,h,i,j), (k,l,m,n,o), and (p,q,r,s,t) have almost the same temperatures of 32, 33, 35, and 38 °C, respectively, and state groups $\{a,f,k,p\}$, $\{b,g,l,q\}$, $\{c,h,m,r\}$, $\{d,i,n,s\}$, and $\{e,j,o,t\}$ have almost the same densities of 0.645, 0.615, 0.528, 0.357, and 0.280 g/cm^3, respectively.

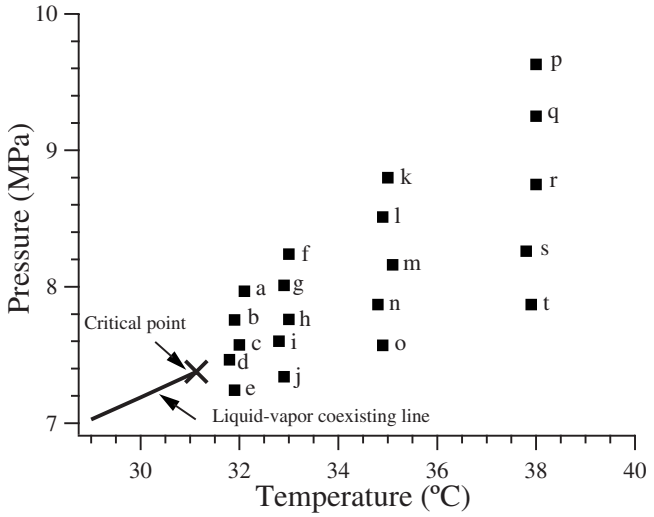

FIG. 1. Thermodynamic states of sc-CO_2 observed in this study. The characters a–t indicate each of the measurement points listed in Table I.

A sample container of sc-CO_2 was made of SUS316 with two sapphire windows. The details of this container and the SCF system were reported in previous papers [17,18]. In the following analysis, SANS data between $Q=0.01$ and 0.5 Å^{-1} were used.

III. RESULTS OF SMALL-ANGLE NEUTRON SCATTERING

Figure 2 shows the SANS intensities at 32 °C; states (a,b,c,d,e). The scattering intensities in the low-Q range increase with decreasing pressure or density in the states a, b, and c, while they decrease with decreasing pressure or density in the states c, d, and e. Therefore, the SANS intensities showed a symmetric change around the state c.

In order to evaluate this change of fluctuation quantitatively, all the observed intensities were analyzed with the OZ equation (1) in following form:

$$\frac{1}{I(Q)} = \frac{1}{I(0)} + \frac{\xi^2}{I(0)} Q^2. \tag{3}$$

This equation means that when we plot $I(Q)^{-1}$ vs Q^2, the inverse intensity is described in a linear form, and then ξ and $I(0)$ can be estimated from the slope and the intercept on the y axis, respectively. Figure 3 shows the so-called OZ plot of

TABLE I. Thermodynamic states of sc-CO_2 in the SANS experiment and the values of Ornstein-Zernike correlation lengths and $I(0)$ which were obtained from the SANS intensities. T, P, and ρ are the temperature, pressure, and density, respectively. ξ is the Ornstein-Zernike correlation length and $I(0)$ is the scattering intensity at $Q=0$. CP is the critical point of CO_2.

	T (°C)	P (MPa)	ρ (g cm^{-3})	ξ (Å)	$I(0)$ (cm^2)
CP	31.1	7.38	0.468		
a	32.1	7.97	0.645	13.2	0.234
b	31.9	7.76	0.619	16.6	0.397
c	32.0	7.57	0.538	41.2	2.605
d	31.8	7.46	0.362	20.3	0.560
e	31.9	7.24	0.279	11.3	0.157
f	33.0	8.24	0.647	12.9	0.219
g	32.9	8.01	0.615	14.7	0.378
h	33.0	7.76	0.524	30.6	1.434
i	32.8	7.60	0.346	18.9	0.491
j	32.9	7.34	0.278	11.2	0.149
k	35.0	8.80	0.646	11.7	0.184
l	34.9	8.51	0.614	13.5	0.269
m	35.1	8.16	0.527	22.1	0.751
n	34.8	7.87	0.355	16.4	0.377
o	34.9	7.57	0.283	10.4	0.138
p	38.0	9.63	0.643	10.8	0.153
q	38.0	9.25	0.613	12.0	0.208
r	38.0	8.75	0.523	16.9	0.435
s	37.8	8.26	0.363	14.2	0.280
t	37.9	7.87	0.278	10.2	0.123

$I(0)/I(Q)^{-1}$ vs Q^2 at 32 °C [here both sides of Eq. (3) were multiplied by $I(0)$ in order to clarify the difference of the slope]. Since all the observed data are well described in the linear form in Fig. 3, it is confirmed that the SANS intensities satisfy the OZ equation in this Q range. The ξ and $I(0)$ obtained at all measurement states are also listed in Table I.

The pressure dependences of ξ and $I(0)$ of all isothermal lines are shown in Figs. 4(a) and 4(b), respectively. It is

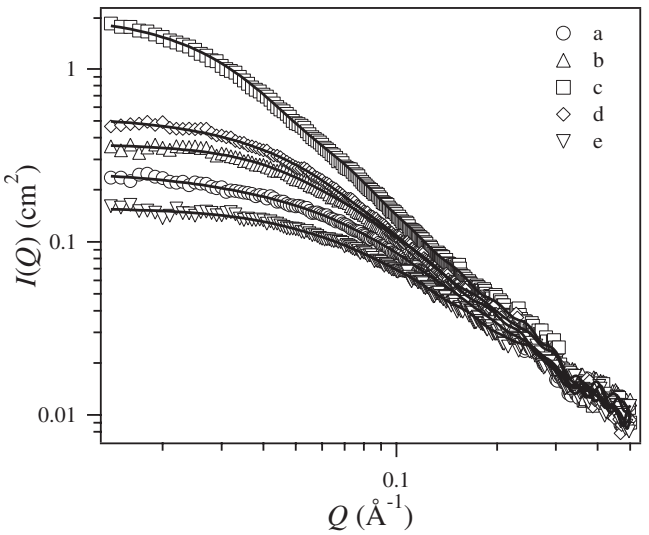

FIG. 2. SANS intensities for sc-CO_2 at 32 °C (states (a,b,c,d,e) in Fig. 1 and Table I). Markers of open circles, triangles, squares, diamonds, and inverted triangles correspond to the states *a*, *b*, *c*, *d*, and *e*, respectively. The solid curves show the results of RMC calculation.

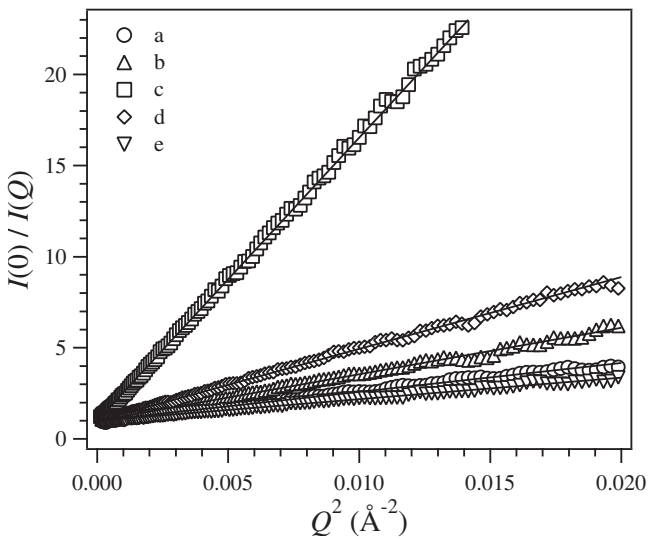

FIG. 3. Ornstein-Zernike plots for SANS data at 32 °C (states *a*–*e*). Markers of open circles, triangles, squares, diamonds, and inverted triangles correspond to the states *a*, *b*, *c*, *d*, and *e*, respectively. The solid thin lines are the fitting results of the Ornstein-Zernike equation (3).

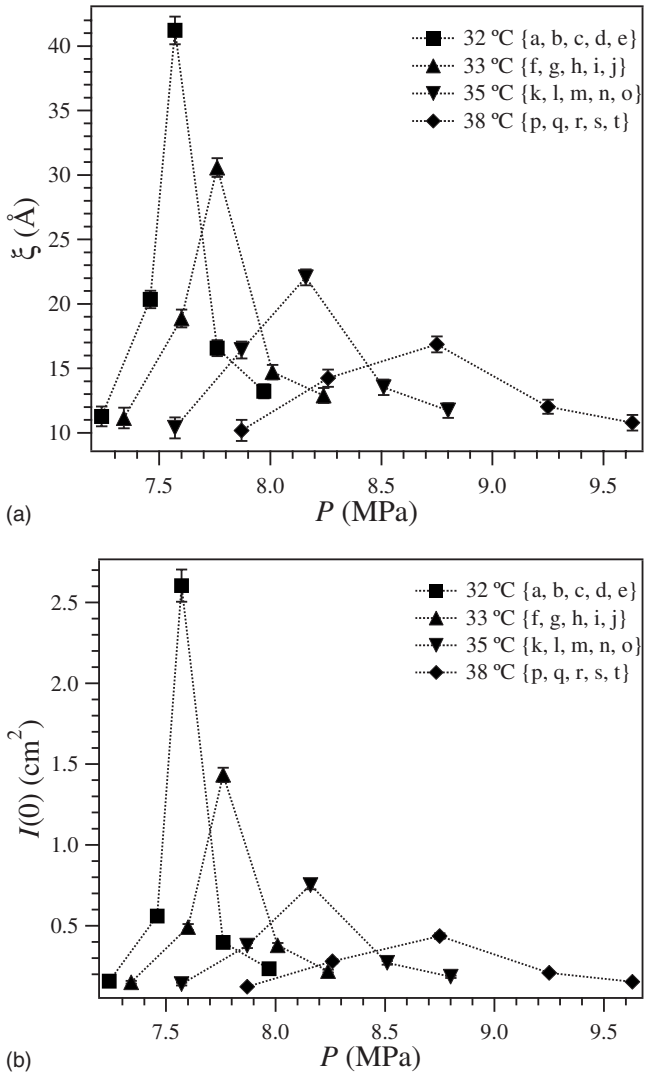

FIG. 4. Pressure dependence of the parameters of the Ornstein-Zernike equation at all isothermal lines. (a) Ornstein-Zernike correlation length ξ, which corresponds to the scale of the density fluctuation; (b) scattering intensity at $Q=0$, $I(0)$, which relates to the magnitude of the density fluctuation. Markers of black squares, triangles, inverted triangles, and diamonds indicate the isothermal lines of 32, 33, 35, and 38 °C, respectively.

apparently confirmed that there exists a locus around the isochoric line of $\{c,h,m,r\}$ where the scale and the magnitude of the density fluctuation become maximal. The locus of the maximal points corresponds to the ridge of the density fluctuation which Nishikawa and co-workers found in previous studies [2–12]. Therefore, it can be judged that the isochoric lines of $\{a,f,k,p\}$ and $\{b,g,l,q\}$ were in the liquidlike phase, $\{d,i,n,s\}$ and $\{e,j,o,t\}$ were in the gaslike phase, and $\{c,h,m,r\}$ was located quite near to the ridge.

IV. REVERSE MONTE CARLO SIMULATION

The traditional OZ equation describes only the deviation of the density from the averaged one. However, the averaged density itself was not in consideration. In order to extract further structural information, we have to include the averaged density into the SANS analysis. For this purpose, it is important to obtain a real-space molecular distribution. Therefore, the RMC method was applied to all the SANS data. The details of the calculation of the RMC calculation and the results are described in this section.

The size of the computational domain of the RMC simulation is determined as $(271.2)^3$ Å^3. It was shown in a previous study that this size is enough to reproduce the largest molecular distribution in this study, i.e., state c [18]. The effective diameter a of a CO_2 molecule is determined to be 3.39 Å with the equation for the critical packing fraction [25,26]

$$\frac{\pi}{6}\rho_{\mathrm{CP}}a^3 = 0.13044, \tag{4}$$

where ρ_{CP} (=0.006 40 Å^{-3}) is the number density of CO_2 molecules at the critical point. The length a exactly corresponds to the intermolecular distance of sc-CO_2 [27–32].

Initially, CO_2 molecules are randomly distributed in the computational domain. The number of molecules was calculated with the density of the state listed in Table I. Then these molecules were moved to reproduce the SANS intensity. The basic algorithm of the RMC method for SANS is exactly the same as in the original RMC computation [20] and was reported in Refs. [18,21]. In the previous study, we used grids on the computational domain, and located the CO_2 molecules only around the grid points [18]. Even though the calculation time was rather shorter, this grid structure caused an artificial oscillation in the obtained pair-distribution function $g(r)$ [18]. In this study, we removed the grid from the domain and located the molecules everywhere except for the excluded volume $\pi a^3/6$ around other molecules. The artificial oscillation in $g(r)$ was expected to be cleared by this improvement.

The calculated scattering curves at 32 °C are additionally shown in Fig. 2. It is apparently confirmed that all the RMC results well reproduce the observed SANS intensities. Figure 5 shows the pair-correlation functions $f_{\mathrm{PC}}(r)=4\pi r^2\rho_0[g(r)-1]$ (ρ_0 is the number density in each state) of states (a,b,c,d,e), which were obtained from the RMC results. As expected above, no artificial oscillation was observed. $f_{\mathrm{PC}}(r)$ means the excess number of molecules at distance r from one CO_2 molecule. Therefore, it directly corresponds to the density fluctuation. $f_{\mathrm{PC}}(r)$ in state c is much higher than those in the other states. This relates to the fact that the observed $I(0)$ in state c was the largest in all the measured states. The convergence distance of $f_{\mathrm{PC}}(r)$ toward zero is also an important parameter indicating the range of the indirect intermolecular correlation [33]. This distance reflects the OZ correlation length ξ, because ξ is a decay parameter of $g(r)$ given as $g(r)-1 \propto \exp(-r/\xi)/r$ in the OZ theorem [33]. The convergence distance of state c where ξ was the largest is about 120 Å. It is extraordinarily larger than in the other states. These facts about $f_{\mathrm{PC}}(r)$ indicate that the RMC results successfully reproduce the real-space molecular distribution of sc-CO_2.

Figures 6(a)–6(e) display the density maps of the real-space molecular distribution of the states (a,b,c,d,e) in a layer with thickness $2a$. In Figs. 6(a) and 6(e), high-density

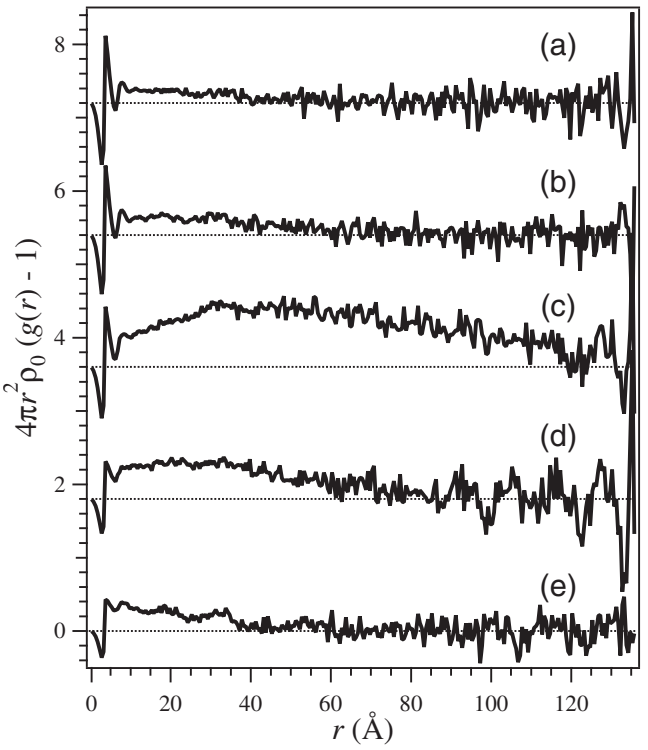

FIG. 5. Pair-correlation function $4\pi r^2\rho_0[g(r)-1]$, of sc-CO_2 at 32 °C (states (a,b,c,d,e)) obtained by the RMC calculation for SANS data.

and low-density areas with small size are observed. On the other hand, high-density and low-density areas with larger size exist in state c. For example, a large high-density area is located around $(x,y)=(200,70)$, and a large low-density area is around $(x,y)=(140,180)$ in Fig. 6(c). In the states b and d, there are fluctuations of intermediate size. This visualization greatly helps us to understand the differences of the fluctuation structures in sc-CO_2 along the isotherm.

V. NUMBER DENSITY DISTRIBUTION OF SCF MOLECULES

In this study, we suggest a statistical analysis method for the obtained real-space molecular distribution in order to obtain detailed information about the density fluctuation structure. The computational domain of the RMC method including the real-space molecular distribution was cut into small cubics of $V=5a\times5a\times5a$ Å^3 ($5a=16.95$ Å). From now on, this cube is called the "cell." Then the number density of molecules in each cell was calculated. Figure 7 shows the number density distributions of states (a,b,c,d,e). As references, the initial distribution of the RMC calculation, i.e., a random distribution, is also displayed. In all states, the standard deviations of the number density distributions were larger than those of the initial distributions. This behavior indicates the existence of density fluctuations because the standard deviation of the number density distribution, $\sigma=(\langle N^2\rangle-\langle N\rangle^2)^{1/2}/V$, corresponds to the magnitude of the density fluctuation. Figure 8 shows the standard deviations of all the observed states. The standard deviations of the states $\{c,h,m,r\}$ on the nearest isochoric line to the ridge are the largest in all isotherms, while the standard deviations are small at states on the two isochoric lines of $\{a,f,k,p\}$ on the high-density side and $\{e,j,o,t\}$ on the low-density side which are located far from the ridge. At the lines of $\{b,g,l,q\}$ and $\{d,i,n,s\}$, the standard deviations have intermediate values. This trend corresponds to the magnitude of the density fluctuation, $I(0)$, of the SANS experiment. Focusing on the isochoric change of the states, the standard deviations decrease with increasing temperature in all lines even though there exist slight exceptions in states b and o. These exceptions come from small deviations of these states from the isochoric lines as shown in Table I. From the consideration above for the standard deviation, the structural feature of the density fluctuation can also be described with a statistical approach. However, the information about the standard deviation indicating the magnitude of the density fluctuation is the same obtained with the traditional OZ equation for SANS data. In order to explain the differences between the liquidlike and gaslike phases, further structural information should be extracted from the real-space molecular distribution.

Looking at the number density distributions shown in Fig. 7 carefully, it is noticeable that some have asymmetric natures. In order to estimate this asymmetry, the skewness of the number density distribution, γ, was calculated. Generally, the skewness γ is defined as the third standardized moment

$$\gamma=\frac{1}{n}\sum_i\frac{(N_i-\langle N\rangle)^3}{V^3\sigma^3}, \tag{5}$$

where N_i is the number of molecules in the ith cell, and n is the number of cells. The skewness has a positive value if the mass of the distribution is concentrated on the left (low-density) side, while, it becomes negative when that is concentrated on the right (high-density) side. Additionally, the skewness becomes zero when the distribution has a symmetric shape.

Figures 9(a) and 9(b) show the obtained skewness of the calculated number density distribution and that of the initial (random) distribution, respectively. As shown in Fig. 9(a), it can be confirmed that the skewness is clearly different depending on the density of the states. When the state is on the isochoric lines of $\{d,i,n,s\}$ and $\{e,j,o,t\}$, the skewness becomes positive. On the other hand, the skewness becomes negative for the states on the isochoric lines of $\{a,f,k,p\}$ and $\{b,g,l,q\}$. This means that the mass of the number density distribution is concentrated on the high-density side when the states are in the liquidlike phase and on the low-density side in states in the gaslike phase. In addition, the skewness of the states on the isochoric line of $\{c,h,m,r\}$, which is the nearest to the ridge, is almost zero, i.e., the distribution is symmetric. When the molecular distribution is random, as shown in Fig. 9(b), the skewness is almost zero without any density dependence. Therefore, the differences of the skewness can be regarded as characteristic of the fluctuation structure at each density. It was suggested from the above consideration that the skewness of the number density distribution

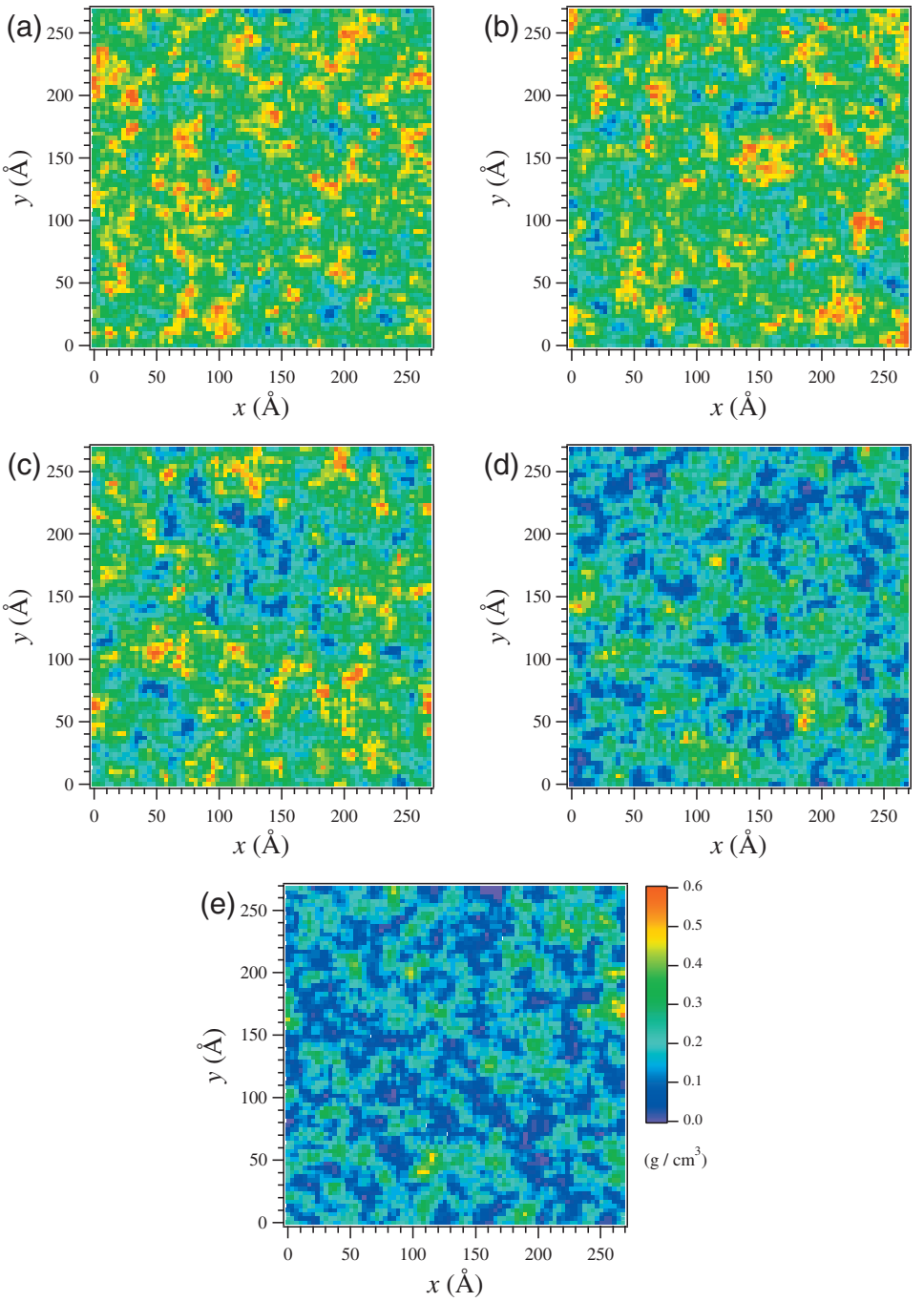

FIG. 6. (Color) Density map of molecular distribution of sc-CO_2 at a certain plane with thickness of $2a$ (=6.78 Å) in the computational domain of the RMC simulation. (a)–(e) correspond to states $a-e$, respectively.

is one of the parameters showing the difference of fluctuation structure between the liquidlike and gaslike phases in SCFs.

VI. ANALYSIS WITH STATISTICAL MECHANICS

In the previous section, it was suggested that the structural difference of the liquidlike and gaslike phases in SCFs can be described by the skewness of the number density distribution. In order to prove the suggestion theoretically, we consider how the skewness is expressed in statistical form in this section.

A cell of the computational domain can be regarded as a system of a statistical ensemble obeying the grand canonical (T,V,μ) distribution. Hence, the number of molecules in a cell can be described with the grand canonical partition function Ξ:

$$\Xi = \sum_j \sum_N e^{-\beta(E_j-\mu N)}, \tag{6}$$

where E_j is the energy of the jth system, μ is the chemical potential, and $\beta=(k_BT)^{-1}$ (k_B is the Boltzmann constant) [34]. With this partition function, the average and the variance of the number of molecules in a cell are expressed as

$$\langle N\rangle = \frac{1}{\beta}\left(\frac{\partial \ln \Xi}{\partial \mu}\right)_{T,V}, \tag{7}$$

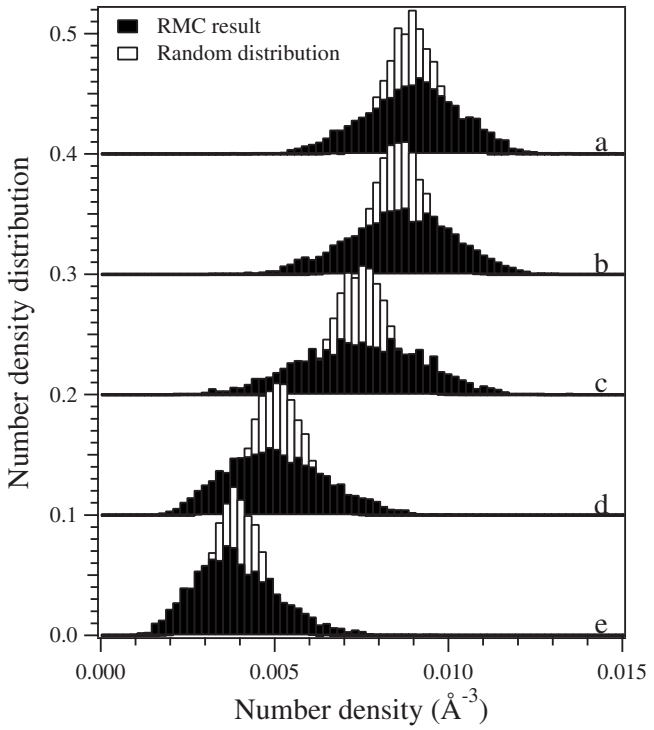

FIG. 7. Number density distribution of sc-CO_2 at 32 °C (states (a,b,c,d,e)). Black bars are distributions of the RMC results. White bars are those of the initial states, i.e., random distributions.

$$\langle N^2\rangle - \langle N\rangle^2 = \frac{1}{\beta^2}\left(\frac{\partial^2 \ln \Xi}{\partial \mu^2}\right)_{T,V}, \tag{8}$$

respectively [34].

The important question is how the skewness is expressed using Ξ. By expanding Eq. (5), we have

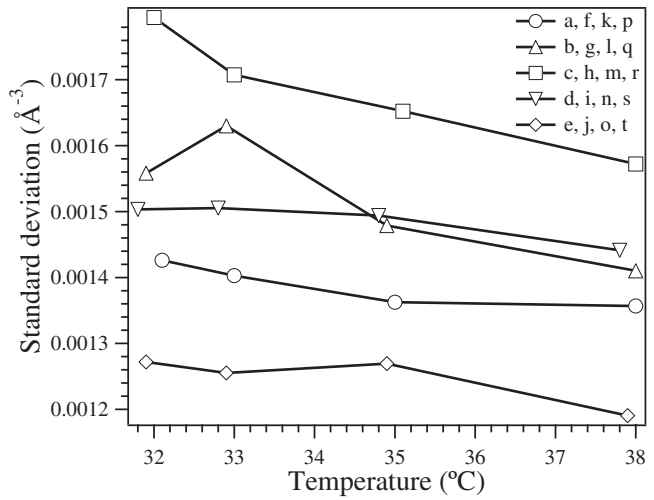

FIG. 8. Standard deviation of the number density distribution of sc-CO_2. Markers of open circles, triangles, squares, diamonds, and inverted triangles correspond to isochoric lines of $\{a,f,k,p\}$, $\{b,g,l,q\}$, $\{c,h,m,r\}$, $\{d,i,n,s\}$, and $\{e,j,o,t\}$, respectively.

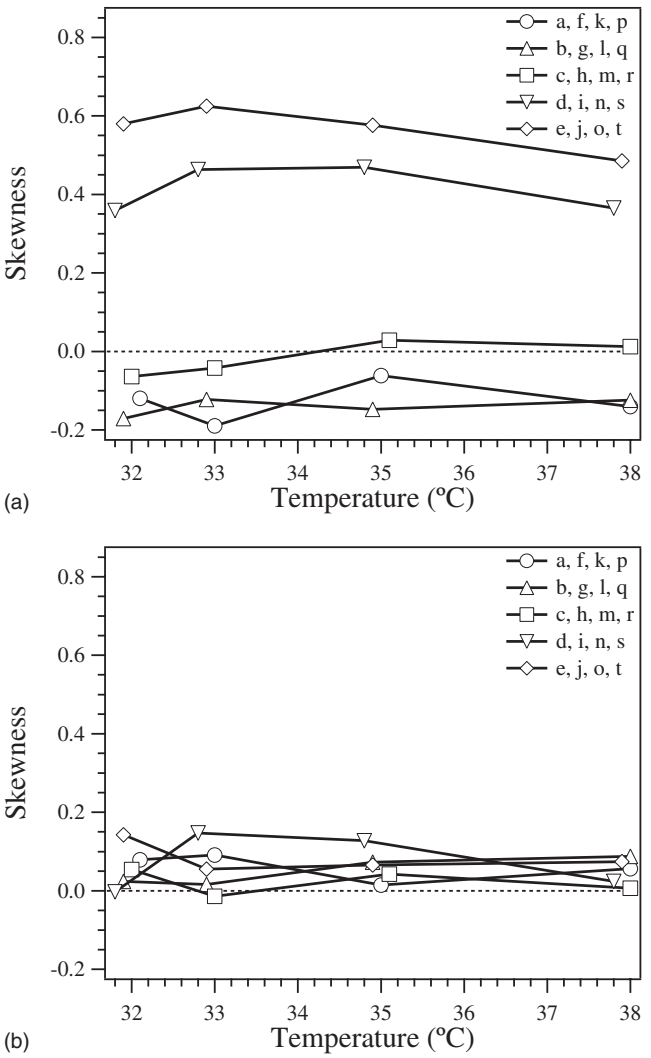

FIG. 9. Skewness of the number density distribution of sc-CO_2. Markers of open circles, triangles, squares, diamonds, and inverted triangles correspond to isochoric lines of $\{a,f,k,p\}$, $\{b,g,l,q\}$, $\{c,h,m,r\}$, $\{d,i,n,s\}$, and $\{e,j,o,t\}$, respectively. (a) RMC results. (b) Initial states (random distribution).

$$\gamma = \frac{1}{n}\sum_i \frac{(N_i - \langle N\rangle)^3}{V^3\sigma^3} = \frac{\langle N^3\rangle - 3\langle N^2\rangle\langle N\rangle + 2\langle N\rangle^3}{V^3\sigma^3}. \tag{9}$$

With a similar form to Eqs. (7) and (8), the third partial differential of $\ln \Xi$ with respect to chemical potential was calculated:

$$\left(\frac{\partial^3 \ln \Xi}{\partial \mu^3}\right)_{T,V} = \frac{1}{\Xi}\left(\frac{\partial^3 \Xi}{\partial \mu^3}\right)_{T,V} - 3\left[\frac{1}{\Xi}\left(\frac{\partial^2 \Xi}{\partial \mu^2}\right)_{T,V}\right] \times \left[\frac{1}{\Xi}\left(\frac{\partial \Xi}{\partial \mu}\right)_{T,V}\right] + 2\left[\frac{1}{\Xi}\left(\frac{\partial \Xi}{\partial \mu}\right)_{T,V}\right]^3 \tag{10}$$

The first, second, and third derivatives of Ξ in Eq. (10) become

$$\frac{1}{\Xi}\left(\frac{\partial}{\partial \mu}\right)_{T,V} = \beta\frac{1}{\Xi}\sum_j \sum_N N e^{-\beta(E_j - \mu N)} = \beta\langle N\rangle, \tag{11}$$

$$\frac{1}{\Xi}\left(\frac{\partial^2\Xi}{\partial\mu^2}\right)_{T,V} = \beta^2\frac{1}{\Xi}\sum_j\sum_N N^2 e^{-\beta(E_j-\mu N)} = \beta^2\langle N^2\rangle, \quad (12)$$

$$\frac{1}{\Xi}\left(\frac{\partial^3\Xi}{\partial\mu^3}\right)_{T,V} = \beta^3\frac{1}{\Xi}\sum_j\sum_N N^3 e^{-\beta(E_j-\mu N)} = \beta^3\langle N^3\rangle, \quad (13)$$

respectively. By substituting Eqs. (11)–(13) into Eq. (10), the third derivative of ln Ξ is expressed in the form

$$\frac{1}{\beta^3}\left(\frac{\partial^3 \ln\Xi}{\partial\mu^3}\right)_{T,V} = \langle N^3\rangle - 3\langle N^2\rangle\langle N\rangle + 2\langle N\rangle^3. \quad (14)$$

Since the right side of the equation is the same as the numerator of Eq. (9), Eq. (14) is the answer indicating the relation between the skewness and the grand partition function Ξ. With Eqs. (8), (9), and (14) the skewness is expressed as the first derivative of the variance,

$$\gamma = \frac{1}{n}\sum_i \frac{(N_i-\langle N\rangle)^3}{V^3\sigma^3} = \frac{1}{\beta V^3\sigma^3}\left(\frac{\partial}{\partial\mu}[\langle N^2\rangle - \langle N\rangle^2]\right)_{T,V}. \quad (15)$$

Furthermore, the Gibbs-Duhem relation for all the sc-CO_2 in the sample container is described as,

$$S_{\mathrm{con}}dT - V_{\mathrm{con}}dP + N_{\mathrm{con}}d\mu = 0, \quad (16)$$

where S_{con}, V_{con}, and N_{con} are the entropy, volume, and number of molecules in the sample container, respectively. By using Eq. (16), the partial differential with respect to chemical potential can be transferred to that of pressure:

$$\left(\frac{\partial}{\partial\mu}\right)_{T,V} = \left(\frac{\partial}{\partial P}\right)_{T,V}\left(\frac{\partial P}{\partial\mu}\right)_{T,V} = \frac{N_{\mathrm{con}}}{V_{\mathrm{con}}}\left(\frac{\partial}{\partial P}\right)_{T,V} = \frac{\langle N\rangle}{V}\left(\frac{\partial}{\partial P}\right)_{T,V}. \quad (17)$$

With Eqs. (15) and (17), the following relation is obtained:

$$\gamma = \frac{1}{n}\sum_i \frac{(N_i-\langle N\rangle)^3}{V^3\sigma^3} = \frac{\langle N\rangle}{\beta V^4\sigma^3}\left(\frac{\partial}{\partial P}[\langle N^2\rangle - \langle N\rangle^2]\right)_{T,V}. \quad (18)$$

Equation (18) indicates that the sign of the differential of the density fluctuation with respect to the pressure is directly connected with the sign of the skewness. Considering our experimental results, the sign of the skewness is determined by whether the slope of Fig. 4(b) is positive or negative. When the state is in the gaslike phase (lower-density side from the ridge), the skewness becomes positive because the magnitude of the density fluctuation increases with increasing pressure. The skewness becomes negative in the state of the liquidlike phase (higher-density side from the ridge) for the same reason. Furthermore, the skewness becomes zero at the states on the ridge. From the above consideration, the skewness obtained from the RMC analysis was theoretically exhibited to be a parameter indicating the difference between the liquidlike and gaslike phases in a SCF.

VII. DISCUSSION

We have shown that the liquidlike and gaslike phases in a SCF can be regarded as states where the skewness is negative and positive, respectively. This understanding is naturally expanded to the general gas-liquid phases for $T<T_c$. When a state in the subcritical region ($T<T_c$) comes close to the line of the first-order phase transition (liquid-gas coexistence line), the density fluctuation generally grows. That is, the density fluctuation increases with decreasing pressure in the liquid phase, while it increases with increasing pressure in the gas phase. This is the same trend as in the supercritical region even though the scale and the magnitude of the density fluctuation are quite small. Therefore, it is predicted with Eq. (18) that the skewness is positive in the gas phase and negative in the liquid phase. We suggest that the skewness is one of the universal parameters by which the liquidlike and gaslike phases are distinguished in both supercritical ($T>T_c$) and subcritical ($T<T_c$) states.

The density fluctuation is connected with the isothermal compressibility κ_T, which is the second derivative of the Gibbs energy G [33]:

$$\langle N^2\rangle - \langle N\rangle^2 = \frac{\langle N\rangle^2 k_B T}{V}\kappa_T, \quad (19)$$

$$\kappa_T = -\frac{1}{V}\left(\frac{\partial^2 G}{\partial P^2}\right)_{T,N}, \quad (20)$$

while the skewness of the number density distribution is the first derivative of the density fluctuation [left side of Eq. (19)], as shown in the last section. Therefore, the skewness corresponds to the third derivative of the Gibbs energy. Generally, higher-order derivatives reflect detailed structural information about the system [35,36]. The analysis method we developed in this study succeeded in extracting information about the third derivative from the SANS data. On the other hand, only the second derivative of the Gibbs energy was evaluated with the traditional OZ equation. This is solid evidence of the progress in analyzing the SANS data.

This innovation was caused by introducing the macroscopic density for the analysis of the SANS data. In other words, the absolute value of the average number of molecules $\langle N\rangle$ in a corresponding volume V was included in our analysis. The OZ equation evaluates the deviation of the number of molecules from the average, $\langle N^2\rangle - \langle N\rangle^2$. However the absolute values of the average number $\langle N\rangle$ are not taken into consideration. The lack of information makes the structural difference between the liquidlike and gaslike phases invisible. On the other hand, our RMC analysis considers the macroscopic density as the number of molecules in the computational domain. Therefore, the absolute value of the local number density can be calculated as the number of molecules in each cell. With both the average number of molecules, $\langle N\rangle$, and the local number of molecules, N, the skewness, the third standardized moment as shown in Eq. (5), can be calculated. By using the further information about the macroscopic density for SANS analysis, we have succeeded in revealing that the skewness is an important parameter for the number density distribution, which shows the structural difference between the liquidlike and gaslike phases in SCFs.

VIII. CONCLUSION

SANS experiments were carried out for sc-CO_2 along isothermal and isochoric lines in order to clarify the structural difference between the liquidlike and gaslike phases in SCFs. The observed scattering intensities were well described with the OZ equation, and the existence of the ridge can be clearly confirmed. With application of the RMC method to the observed SANS intensity, the real-space molecular distribution was successfully obtained. The number density distributions of the CO_2 molecules for all states were calculated using the results of the RMC simulation. The standard deviation of the number density distribution shows good agreement with the experimental results. The skewness of each distribution was also calculated in order to evaluate its asymmetric nature. The skewness clearly showed the differences of the molecular distribution structure between the liquidlike and gaslike phases. It becomes positive in states in the gaslike phase, negative in the liquidlike phase, and almost zero at the states on the nearest isochoric line to the ridge. It was proved with simple equations of statistical mechanics that the skewness is described as the first partial differential of the magnitude of the density fluctuation with respect to the pressure. We conclude that the molecular distribution structures of the liquidlike and gaslike phases can be distinguished using the skewness of the number density distribution, obtained by RMC analysis for SANS data.

ACKNOWLEDGMENTS

The authors wishes to thank Takao Mitsui for kindy help in the SANS experiment, and Dr. Laszlo Pusztai for useful discussions on reverse Monte Carlo calculations. The work was partially supported by a Grant-in-Aid for Creative Scientific Research (Grant No. 16GS0417). M.S. is supported by a Grant-in-Aid for Scientific Research of the Ministry of Education, Science and Culture, Japan (Grant No. 19540427).

[1] S. C. Tucker, Chem. Rev. (Washington, D.C.) **99**, 391 (1999).
[2] K. Nishikawa and I. Tanaka, Chem. Phys. Lett. **244**, 149 (1995).
[3] K. Nishikawa, I. Tanaka, and Y. Amemiya, J. Phys. Chem. **100**, 418 (1996).
[4] K. Nishikawa and T. Morita, J. Phys. Chem. B **101**, 1413 (1997).
[5] K. Nishikawa and T. Morita, J. Supercrit. Fluids **13**, 143 (1998).
[6] K. Nishikawa, and T. Morita, Chem. Phys. Lett. **316**, 238 (2000).
[7] T. Morita, K. Kusano, H. Ochiai, K. Saitow, and K. Nishikawa, J. Chem. Phys. **112**, 4203 (2000).
[8] K. Nishikawa, H. Ochiai, K. Saitow, and T. Morita, Chem. Phys. **286**, 421 (2003).
[9] K. Nishikawa, K. Kusano, A. A. Arai, and T. Morita, J. Chem. Phys. **118**, 1341 (2003).
[10] A. A. Arai, T. Morita, and K. Nishikawa, J. Chem. Phys. **119**, 1502 (2003).
[11] K. Nishikawa, A. A. Arai, and T. Morita, J. Supercrit. Fluids **30**, 249 (2004).
[12] A. A. Arai, T. Morita, and K. Nishikawa, Fluid Phase Equilib. **252**, 114 (2007).
[13] M. Kamiya, K. Muroki, and M. Uematsu, J. Chem. Thermodyn. **27**, 337 (1995).
[14] C. A. Eckert, D. H. Ziger, K. P. Johnston, and S. Kim, J. Phys. Chem. **90**, 2738 (1986).
[15] E. F. Carome, C. B. Cykowski, J. F. Havlice, and D. A. Swyt, Physica (Amsterdam) **38**, 307 (1968).
[16] Z. Chen, K. Tozaki, and K. Nishikawa, Jpn. J. Appl. Phys., Part 1 **38**, 6840 (1999).
[17] M. Sugiyama, K. Hara, M. Hino, M. Annaka, T. Saito, and T. Fukunaga, Trans. Mater. Res. Soc. Jpn. **28**, 1013 (2003).
[18] T. Sato, M. Sugiyama, M. Misawa, S. Takata, T. Otomo, K. Itoh, K. Mori, and T. Fukunaga, J. Phys.: Condens. Matter **20**, 101203 (2008).
[19] T. Sato, M. Sugiyama, M. Misawa, K. Hamada, K. Itoh, K. Mori, and T. Fukunaga, J. Mol. Liq. (to be published).
[20] R. L. McGreevy and L. Pusztai, Mol. Simul. **1**, 359 (1998).
[21] M. Misawa, J. Chem. Phys. **116**, 8463 (2002).
[22] M. Misawa, I. Dairoku, A. Homma, Y. Yamada, T. Sato, K. Maruyama, K. Mori, S. Suzuki, and T. Otomo, J. Chem. Phys. **121**, 4716 (2004).
[23] T. Otomo, M. Furusaka, S. Satoh, S. Itoh, T. Adachi, S. Shimizu, and M. Takeda, J. Phys. Chem. Solids **60**, 1579 (1999).
[24] R. Span and W. Wagner, J. Phys. Chem. Ref. Data **25**, 1509 (1996).
[25] D. A. Young and B. J. Alder, Phys. Rev. A **3**, 364 (1971).
[26] M. Misawa, J. Chem. Phys. **93**, 8401 (1990).
[27] K. Nishikawa and M. Takematsu, Chem. Phys. Lett. **226**, 359 (1994).
[28] R. Ishii, S. Okazaki, I. Okada, M. Furusaka, N. Watanabe, M. Misawa, and T. Fukunaga, Chem. Phys. Lett. **240**, 84 (1995).
[29] R. Ishii, S. Okazaki, O. Odawara, I. Okada, M. Misawa, and T. Fukunaga, Fluid Phase Equilib. **104**, 291 (1995).
[30] R. Ishii, S. Okazaki, I. Okada, M. Furusaka, N. Watanabe, M. Misawa, T. Fukunaga, J. Chem. Phys. **105**, 7011 (1996).
[31] S. Chiappini, M. Nardone, F. P. Ricci, and M. C. Bellissent-Funel, Mol. Phys. **89**, 975 (1996).
[32] T. Morita, K. Nishikawa, M. Takematsu, H. Iida, S. Furutaka, J. Phys. Chem. B **101**, 7158 (1997).
[33] H. E. Stanley, *Introduction to Phase Transitions and Critical Phenomena* (Clarendon Press, Oxford, 1971).
[34] W. Greiner, L. Neise, and H. Stöcker *Thermodynamics and Statistical Mechanics* (Springer, Berlin, 1995).
[35] Y. Koga, J. Phys. Chem. **100**, 5172 (1996).
[36] L. G. Hepler, Can. J. Chem. **47**, 4613 (1969).